

Dynamical Selection in Emergent Fermionic Pairing

R. A. Barankov and L. S. Levitov

Department of Physics, Massachusetts Institute of Technology, 77 Massachusetts Ave, Cambridge, MA 02139

(June 16, 2021)

We consider evolution of a Fermi gas in the presence of a time-dependent BCS interaction. The pairing amplitude in the emergent BCS state is found to be an oscillatory function of time with predictable characteristics. The interplay of linear instability of the unpaired state and nonlinear interactions selects periodic soliton trains of a specific form, described by the Jacobi elliptic function dn . While the parameters of the soliton train, such as the period, amplitude, and time lag, fluctuate among different realizations, the elliptic function form remains robust. The parameter variation is accounted for by the fluctuations of particle distribution in the initial unpaired state.

Nonequilibrium effects in superconducting systems are usually described using the notion of local equilibrium and quasiparticle distribution [1,2], embodied in the time-dependent Ginzburg-Landau equation [3] or the kinetic equation [4]. The recently studied problem of fast time dynamics in emergent fermionic pairing [5] describing the onset of BCS pairing triggered by an abrupt change of interaction lies somewhat outside this classification. The new aspect of this problem is the absence of a meaningful notion of quasiparticle spectrum. Instead, individual Cooper pair states evolve in a coherent, collisionless fashion [6–9] *independently* of the order parameter. The ensuing interesting many-body evolution reflects the system inability to transit adiabatically between the unpaired and paired states due to their vanishing overlap. The oscillatory mode [5] can be viewed as Bloch precession of the pair states in an effective magnetic field defined in terms of the pairing function.

Tunable time-dependent pairing interaction can be realized experimentally in ultracold Fermi gases [10–13]. Fermionic pairing and superfluidity in these systems have been demonstrated recently using magnetically tunable Feshbach resonances [14–16]. In these systems, by varying the magnetic field detuning from resonance, both the strength and the sign of inter-particle interaction can be changed on a time scale shorter than the intrinsic times of fermions, set by E_F or the elastic collision rate. In Refs. [18,20,21] the picture of time-dependent pairing [5] was extended to the problem of resonant atom-molecule coupling near a Feshbach resonance.

Another interesting class of tunable systems are the hybrid semiconductor-superconductor (S/Sm/S) and SNS structures [24–28] with proximity-induced Josephson effect. In the S/Sm/S systems [24,25], the superfluid density and Josephson critical current can be tuned by electric field applied on the gates to the semiconductor. Similarly, the SNS structures [26–28] are tunable by current applied to the normal region.

Superconductor dynamics is controlled by several kinetic time scales [2]. The most important for us is the collisionless regime [6–9] characterized by the time

$$\tau_{\Delta} = \hbar/\Delta \quad (1)$$

with Δ the equilibrium BCS gap. The time τ_{Δ} manifests

itself in the BCS instability growth rate [7–9] at T away from T_c , as well as in the frequency of pairing amplitude oscillations [6]. Another time scale is set by the Landau Fermi liquid elastic collision time, $\tau_{\text{el}}^{-1} \propto \max[\epsilon^2, T^2]$ with ϵ the energy relative to E_F . For typical energy $\epsilon \simeq \Delta$, in the weak coupling regime $\Delta \ll E_F$, we estimate $\tau_{\text{el}} \gg \tau_{\Delta}$. For slowly varying interaction, the kinetic equation [4], or the time-dependent Ginzburg-Landau equation [3] can be employed. In contrast, here we are interested in the situation when the interaction is turned on abruptly on the scale τ_{Δ} , so that the hierarchy of times is

$$\tau_0 \ll \tau_{\Delta} \ll \tau_{\text{el}}, \quad (2)$$

where τ_0 describes the interaction time dependence. In this case, the time interval $0 < t \lesssim \tau_{\text{el}}$ is controlled by coherent pair dynamics, while energy relaxation can be ignored. This regime can be described by the truncated BCS Hamiltonian, which accounts for coherent Cooper pair transitions $(\mathbf{p}, -\mathbf{p}) \rightarrow (\mathbf{p}', -\mathbf{p}')$, ignoring other, more slow, processes of quasiparticle scattering. In this article we study the resulting collisionless evolution, using a combination of analytical and numerical methods.

The time domain picture of BCS pairing buildup, proposed in Ref. [5], involves dynamics of individual pair states, selfconsistently coupled to the pairing amplitude. The latter exhibits unharmonic oscillations, undamped at $t < \tau_{\text{el}}$. While several recent publications agree in general with this scenario [19–22], some of the issues remain unsettled. Ref. [19] describes a simulation of the collisionless BCS dynamics exhibiting a damped oscillatory time dependence, with the damping of unspecified origin. These results, as well as those of Ref. [23], are clearly different from the behavior found in Ref. [5]. The most probable origin of the discrepancy, in our view, is due to the numerical method [19].

Below we provide extensive numerical evidence which confirms the conclusions of Ref. [5]. We show that the mean field solutions, the soliton trains described by elliptic dn function, are singled out by the BCS evolution, and appear for generic initial conditions in a stable and robust way. Estimates of noise made in Sec.IV show that the mean field theory approach holds when the level spacing in a relevant volume is small enough. Our analysis

indicates that the mean field results describe the dynamics of $|\Delta|$ in a wide temperature range not only in a finite, but also, locally, in an infinite system.

The physical reason for a specific solution to be selected by pairing dynamics is due to the properties of the BCS instability. Linearization over the unpaired state of a Fermi gas in a finite system, discussed in Sec.I, shows that, modulo phase degeneracy, there is just one unstable normal mode corresponding to perturbation growth, while other modes do not grow. As a result, although the initial state is perturbed by thermal fluctuations in a completely random fashion, the BCS dynamics amplifies only one specific perturbation leading to an oscillatory time dependence with predictable characteristics.

I. BCS INSTABILITY OF THE UNPAIRED FERMION GAS

The evolution of the Fermi gas with time-varying pairing coupling can be described by the BCS Hamiltonian

$$\mathcal{H} = \sum_{\mathbf{p}, \sigma} \epsilon_{\mathbf{p}} a_{\mathbf{p}, \sigma}^{\dagger} a_{\mathbf{p}, \sigma} - \frac{\lambda(t)}{2} \sum_{\mathbf{p}, \mathbf{q}} a_{\mathbf{p}, \uparrow}^{\dagger} a_{-\mathbf{p}, \downarrow}^{\dagger} a_{-\mathbf{q}, \downarrow} a_{\mathbf{q}, \uparrow}, \quad (3)$$

where $a_{\mathbf{p}, \sigma}, a_{\mathbf{p}, \sigma}^{\dagger}$ are the canonical fermion operators, and $\sigma = \uparrow, \downarrow$ is generalized spin. The time dependence of λ , as well as the resulting time dependence of the system state, is assumed to be fast on the scale of quasiparticle elastic collisions and energy relaxation, τ_{el} , allowing us to ignore the latter and consider the coherent dynamics defined by (3). The simplest time dependence which we shall be most interested in, is described by the coupling turned on abruptly, from $\lambda(t < 0) = 0$ to $\lambda(t > 0) = \lambda$.

The interaction switching, while abrupt and nonadiabatic, must also be gentle enough not to overheat the Fermi system. The analysis of energy production due to two-particle scattering in the presence of time-dependent coupling, described in Appendix, obtains an estimate for the effective temperature

$$T_{\text{eff}}^2 = \lambda^2 \nu^3 / \tau_0^3. \quad (4)$$

The ‘no overheat’ condition $T_{\text{eff}} \ll \Delta_0$ can thus be stated as $E_F \tau_0 \gg (\lambda n / \Delta_0)^{2/3}$, which is compatible with the nonadiabaticity requirement $\tau_0 \ll \tau_{\Delta}$.

Our treatment of the problem (3) will focus on the time-dependent generalization of the BCS state [5]

$$|\Psi(t)\rangle = \prod_{\mathbf{p}} \left(u_{\mathbf{p}}(t) + v_{\mathbf{p}}(t) a_{\mathbf{p}, \uparrow}^{\dagger} a_{-\mathbf{p}, \downarrow}^{\dagger} \right) |0\rangle. \quad (5)$$

The Bogoliubov mean field approach, which gives a state of the form (5), relies on the ‘infinite range’ form of the pairing interaction in (3) owing to equal coupling strength of all $(\mathbf{p}, -\mathbf{p}), (\mathbf{q}, -\mathbf{q})$. Since the latter does not depend on the system being in equilibrium, one can introduce a time-dependent mean field pairing function

$$\Delta(t) = \lambda \sum_{\mathbf{p}} u_{\mathbf{p}}(t) v_{\mathbf{p}}^*(t). \quad (6)$$

The amplitudes $u_{\mathbf{p}}(t), v_{\mathbf{p}}(t)$ can be obtained from the Bogoliubov-deGennes equation

$$i\partial_t \begin{pmatrix} u_{\mathbf{p}} \\ v_{\mathbf{p}} \end{pmatrix} = \begin{pmatrix} \epsilon_{\mathbf{p}} & \Delta \\ \Delta^* & -\epsilon_{\mathbf{p}} \end{pmatrix} \begin{pmatrix} u_{\mathbf{p}} \\ v_{\mathbf{p}} \end{pmatrix}, \quad (7)$$

solved together with the selfconsistency condition (6).

We recall that the unpaired state is a selfconsistent, albeit unstable, solution of Eqs. (7),(6) with $\Delta = 0, T = 0$:

$$u_{\mathbf{p}}^{(0)}(t) = e^{-i\epsilon_{\mathbf{p}} t} \theta(\epsilon_{\mathbf{p}}), \quad v_{\mathbf{p}}^{(0)}(t) = e^{i\phi_{\mathbf{p}}} e^{i\epsilon_{\mathbf{p}} t} \theta(-\epsilon_{\mathbf{p}}), \quad (8)$$

with $\phi_{\mathbf{p}}$ a random phase. The stability analysis [8] shows that the deviation from the unpaired state grows as $\Delta(t) \propto e^{\gamma t} e^{-i\omega t}$, with linearized amplitudes

$$\delta u_{\mathbf{p}}(t) = \frac{\Delta(t) v_{\mathbf{p}}^{(0)}(t)}{i\gamma - 2\epsilon_{\mathbf{p}} + \omega}, \quad \delta v_{\mathbf{p}}(t) = \frac{\Delta^*(t) u_{\mathbf{p}}^{(0)}(t)}{i\gamma + 2\epsilon_{\mathbf{p}} - \omega}. \quad (9)$$

The growth exponent γ and the constant ω , combined into a complex number $\zeta = \omega + i\gamma$, are defined by the selfconsistency condition of the linearized problem:

$$1 = \lambda \sum_{\mathbf{p}} \frac{\text{sgn } \epsilon_{\mathbf{p}}}{2\epsilon_{\mathbf{p}} - \zeta}. \quad (10)$$

This equation has a pair of complex conjugate solutions ζ, ζ^* . From the similarity between Eq. (10) and the BCS gap equation one expects the exponent γ to be close to the BCS gap value Δ_0 in equilibrium, in which case the time constant $\tau_{\Delta} = \gamma^{-1}$ for initial pairing buildup is of the order of Δ_0^{-1} .

It will be convenient for us to introduce here the constant density of states approximation,

$$\nu(\epsilon_{\mathbf{p}}) = \begin{cases} \nu_0, & |\epsilon_{\mathbf{p}}| < \frac{1}{2}W \\ 0, & \text{else} \end{cases}, \quad (11)$$

used throughout this article. In our numerical study we use a total $N \gg 1$ equally spaced discrete states distributed evenly in a finite size band,

$$-W/2 \leq \epsilon_{\mathbf{p}} \leq W/2, \quad (12)$$

with the level spacing $\delta\epsilon = W/N$. Although somewhat artificial, the model (12) introduces a convenient simplification due to the particle-hole symmetry. In this case, the chemical potential is locked at $\epsilon = 0$ independent of the interaction strength. As a result, the instability problem (18) possesses an eigenvalue with a purely imaginary $\zeta = i\gamma$, satisfying

$$1 = \lambda \sum_{\mathbf{p}} \frac{2|\epsilon_{\mathbf{p}}|}{4\epsilon_{\mathbf{p}}^2 + \gamma^2}, \quad (13)$$

and $\omega = 0$. Interestingly, if the bandwidth W is much larger than the BCS gap Δ_0 at $T = 0$, the value of the exponent γ obtained from (10) coincides with Δ_0 . Indeed, Eq.(13) in this case gives

$$1 = 2\lambda\nu_0 \int_0^{W/2} \frac{2\epsilon d\epsilon}{4\epsilon^2 + \gamma^2} = \frac{1}{2}\lambda\nu_0 \ln \frac{W^2 + \gamma^2}{\gamma^2} \quad (14)$$

This equation is reminiscent of the BCS gap equation

$$1 = \frac{1}{2}\lambda \int_{-W/2}^{W/2} \frac{d\epsilon}{\sqrt{\epsilon^2 + \Delta_0^2}} = \lambda\nu_0 \sinh^{-1} \frac{W}{2\Delta_0},$$

becoming identical to it in the weak coupling limit of fermion energy band wide compared to the gap, $W \gg \gamma, \Delta_0$ [cf. Eq.(41) below]. The condition $\omega = 0$ is violated in the absence of particle-hole symmetry. The equality $\gamma = \Delta_0$ holds only at $T = 0$.

Let us briefly discuss how the analysis is modified in the case of a discrete spectrum (12). With the sum in Eq.(10) running over N levels, we obtain a polynomial of order N , having total N roots. Simple analysis shows that $N - 2$ roots are real and the remaining two are a complex conjugate pair ζ, ζ^* with values close to that obtained for continuous spectrum. Accordingly, only the normal modes corresponding to ζ, ζ^* are relevant for the instability, while the other $N - 2$ modes correspond to the perturbations which do not grow and remain small. This conclusion is valid only at the times described by the linearized BCS dynamics. The situation at longer times, which is more delicate, will be discussed below.

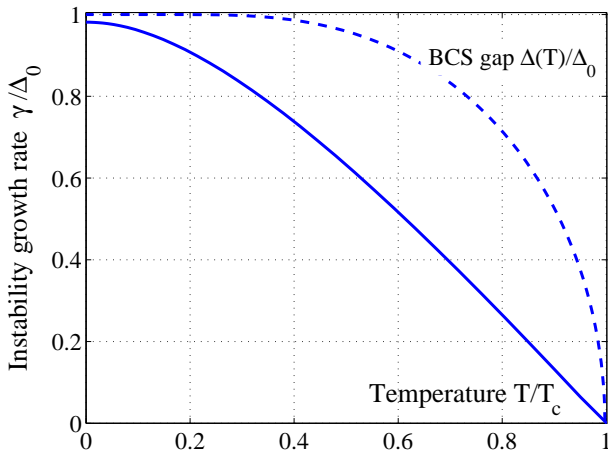


FIG. 1. Temperature dependence of the BCS instability growth rate γ as obtained from Eq.(18) for the constant density of states model (11), (12) with the coupling λ such that $\Delta_0/W = 1/5$. Note that γ coincides with the BCS gap Δ_0 at $T = 0$, up to a correction small as $(\gamma/W)^2$ at large bandwidth W . Near $T_c = \pi e^{-C} \Delta_0 \simeq 1.764\Delta_0$, the exponent γ vanishes linearly in $T_c - T$.

Let us now consider the instability at finite temperature. The initial state describing Fermi gas at $T > 0$ can be tentatively chosen as

$$\prod_{\mathbf{p}} \left(u_{\mathbf{p}} + c_{\mathbf{p}} a_{\mathbf{p},\uparrow}^+ + c'_{\mathbf{p}} a_{-\mathbf{p},\downarrow}^+ + v_{\mathbf{p}} a_{\mathbf{p},\uparrow}^+ a_{-\mathbf{p},\downarrow}^+ \right) |0\rangle, \quad (15)$$

where $u_{\mathbf{p}}, c_{\mathbf{p}}, c'_{\mathbf{p}}, v_{\mathbf{p}}$ equal zero or one depending on the occupancy: $(u_{\mathbf{p}}, c_{\mathbf{p}}, c'_{\mathbf{p}}, v_{\mathbf{p}}) = (1, 0, 0, 0), \dots, (0, 0, 0, 1)$. The average values are given by occupation probabilities:

$$\overline{|u_{\mathbf{p}}|^2} = (1 - n_{\mathbf{p}})^2, \quad \overline{|v_{\mathbf{p}}|^2} = n_{\mathbf{p}}^2, \quad \overline{|c_{\mathbf{p}}|^2} = \overline{|c'_{\mathbf{p}}|^2} = n_{\mathbf{p}}(1 - n_{\mathbf{p}}),$$

where $n_{\mathbf{p}} = 1/(e^{\beta\epsilon_{\mathbf{p}}} + 1)$ is the Fermi function, and the quantities $n_{\mathbf{p}}^2, n_{\mathbf{p}}(1 - n_{\mathbf{p}})$ and $(1 - n_{\mathbf{p}})^2$ describe double, single and zero occupancy probability of the two-fermion states $(\mathbf{p}, -\mathbf{p})$ in the unpaired system. As we argue below, while the product state (15), written as a finite temperature generalization of (5), is not the most general fermion state, it is adequate for our problem.

The product state (15) is suitable for simulation, since Bogoliubov-deGennes dynamics (7) couples only $u_{\mathbf{p}}$ and $v_{\mathbf{p}}$ independently for each \mathbf{p} , preserving the product form. At the same time, the parts of (15) with single occupancy are decoupled from the collisionless pair dynamics (3). Indeed, the Hamiltonian (3) gives zero when applied to singly occupied pair states $a_{\mathbf{k},\uparrow}^+|0\rangle, a_{-\mathbf{k},\downarrow}^+|0\rangle$, irrespective of the occupancy of other pair states. One can thus identify a subspace in the full Hilbert space, which is spanned by all combinations of pair states of occupancy zero and two. The latter have the form

$$|\psi\rangle_{\text{general}} = \prod_{\mathbf{k}}' a_{\mathbf{k},\uparrow}^+ a_{-\mathbf{k},\downarrow}^+ |0\rangle, \quad (16)$$

with the product taken over the states $(\mathbf{k}, -\mathbf{k})$ of occupancy two whereby the states of occupancy one are excluded from the vacuum $|0\rangle$. The states (16) are mapped by (3) onto the states of a similar form, thereby defining a full representation of the Hamiltonian.

Fortunately, one can bypass the combinatorics of (16) and simplify the state by employing Bogoliubov mean field approach which is exact for the Hamiltonian (3). In the mean field framework, the general state is replaced by a product state. Indeed, since the pairing amplitude $\Delta(t)$, describing cumulative effect of all pairs, is a c-number, the dynamics (7) does not generate correlations between different pair states. At the same time, any correlations present at $t = 0$ are dephased by the dynamics itself, described by time-dependent 2×2 evolution matrices, different for each pair $(\mathbf{p}, -\mathbf{p})$. This argument, which will be refined in Sec.V, allows to replace the general states (16) by a simpler state of the product form (15) with $c_{\mathbf{p}} = c'_{\mathbf{p}} = 0$. On a mean field level, the correlations between different $(\mathbf{p}, -\mathbf{p}), (\mathbf{k}, -\mathbf{k})$ do not matter.

The effect of Pauli blocking which eliminates the states of occupancy one can be taken into account by going back to the $T = 0$ state (5) with $u_{\mathbf{p}}$ and $v_{\mathbf{p}}$ chosen as

$$u_{\mathbf{p}}^{(0)}(t) = e^{-i\epsilon_{\mathbf{p}}t}(1 - n_{\mathbf{p}}), \quad v_{\mathbf{p}}^{(0)}(t) = e^{i\phi_{\mathbf{p}}} e^{i\epsilon_{\mathbf{p}}t} n_{\mathbf{p}}, \quad (17)$$

with random phase $\phi_{\mathbf{p}}$. The reduced norm $|u_{\mathbf{p}}|^2 + |v_{\mathbf{p}}|^2 = n_{\mathbf{p}}^2 + (1 - n_{\mathbf{p}})^2 < 1$ reflects that at finite temperature some pair states, populated by just one particle, are decoupled from the dynamics. Near the Fermi level, at $|\epsilon_{\mathbf{p}}| \ll T$, the two-particle states with double or zero occupancy have the probability 1/4 each, so that $|u_{\mathbf{p}}|^2 + |v_{\mathbf{p}}|^2 = 1/2$. Outside this interval, $|\epsilon_{\mathbf{p}}| \geq T$, the blocking is practically absent and the norm approaches one. Below we shall use the state (5) with $u_{\mathbf{p}}, v_{\mathbf{p}}$ given by (17) as initial condition for the simulation.

The choice (17), while somewhat *ad hoc*, has an additional advantage over choosing $u_{\mathbf{p}} = 1, 0, v_{\mathbf{p}} = 0, 1$. With both $u_{\mathbf{p}}$ and $v_{\mathbf{p}}$ nonzero with random relative phase, the state (5) exhibits pairing fluctuations, providing a “seed” for the BCS instability in the simulation. The results of the latter indicate that this choice of the initial state is general enough for the instability to fully play out. As we shall see in Sec.V, where a spin 1/2 formulation of BCS dynamics is discussed, $u_{\mathbf{p}}$ and $v_{\mathbf{p}}$ can be understood as a two-component spinor. This means that the state of the entire system can indeed be chosen in the product form, with the initial values $u_{\mathbf{p}}, v_{\mathbf{p}}$ having random modulus, not just phase. This difference, however, is inessential, since the modulus of $u_{\mathbf{p}}, v_{\mathbf{p}}$ is quickly randomized by the dynamics itself.

Returning to the analysis of the instability, linearization of (7) over the finite temperature state (17) obtains a time-dependent perturbation of the form Eq.(9), and a generalization of Eq.(10), with $\text{sgn } \epsilon_{\mathbf{p}}$ replaced by

$$\overline{|u_{\mathbf{p}}^{(0)}|^2} - \overline{|v_{\mathbf{p}}^{(0)}|^2} = 1 - 2n_{\mathbf{p}} = \tanh \frac{1}{2} \beta \epsilon_{\mathbf{p}}.$$

The resulting equation,

$$1 = \lambda \sum_{\mathbf{p}} \frac{1 - 2n_{\mathbf{p}}}{2\epsilon_{\mathbf{p}} - \zeta}, \quad \Delta(t) \propto e^{-i\zeta t}, \quad (18)$$

has nonzero solutions ζ, ζ^* below the BCS transition, $T < T_c$, which are purely imaginary, $\zeta, \zeta^* = \pm i\gamma$, in the case of particle-hole symmetry (11), (12). The growth exponent γ vanishes as $T \rightarrow T_c$, as shown in Fig.1. This can be verified by noting that Eq.(18) yields infinitesimally small γ at $T = T_c$, since at $\zeta = 0$ it becomes identical to the BCS equation for T_c .

Having established the form of the unstable mode (9) obtained from linearization, let us now estimate the time range for which this analysis is accurate. The denominator in Eq.(9) is larger than the numerator as long as $\Delta(t) \lesssim \gamma$, with $\gamma \approx \Delta(T)$, the BCS gap. The initial value $\eta = \Delta(t=0)$, nonzero due to fluctuations in the unpaired Fermi system, is small in $1/N$:

$$\eta = \lambda \sum_{\mathbf{p}} u_{\mathbf{p}} v_{\mathbf{p}}^* = \lambda \sum_{\mathbf{p}} n_{\mathbf{p}} (1 - n_{\mathbf{p}}) e^{i\phi_{\mathbf{p}}}. \quad (19)$$

The sum (19) is controlled by about $T/\delta\epsilon$ terms with $|\epsilon_{\mathbf{p}}| \lesssim T$, uncorrelated in phase. From the central limit theorem argument, we estimate $\eta \simeq \lambda \nu \sqrt{T \delta\epsilon}$ by order

of magnitude. The condition $\Delta(t) \lesssim \gamma$, with exponentially growing $\Delta(t) = \eta e^{\gamma t}$, defines the time interval $0 < t \lesssim \gamma^{-1} \ln(\gamma/\eta)$ in which the evolution is described by the linearized problem.

Our aim will be to gain insight in the behavior at later times. We rely on the nondissipative character of the Bogoliubov-deGennes dynamics (7),(6), manifest, for instance, in the energy $E = \langle \Psi(t) | \mathcal{H} | \Psi(t) \rangle$ conservation throughout the evolution. Since for the unpaired state the energy exceeds its value in the ground state by the BCS condensation energy, the equilibrium cannot be reached without collisions. Eqs.(7),(6) hold at times shorter than quasiparticle thermalization time τ_{el} . For temperatures away from T_c , the time τ_{el} , evaluated at $\epsilon \simeq \Delta_0$, is long compared to the instability growth time,

$$\tau_{\text{el}} \gg \gamma^{-1}. \quad (20)$$

This means that the linear instability phase is followed by a long *collisionless nonlinear phase*. Below we show that the evolution governed by Eqs.(7),(6) is described by soliton-like pulses in $\Delta(t)$. We obtain a family of exact solutions of the form of single solitons and soliton trains, and compare it with simulations.

We briefly note that the importance of coherent dynamics of individual Cooper pairs (5) in the time evolution of a paired state has been understood a long time ago in the context of the discussion of the validity of the time-dependent Ginzburg-Landau equation approach [7,8,3]. It has been pointed out by Gorkov and Eliashberg [3] that the time-dependent pairing function Δ is generally insufficient to describe the evolution. For such a description to be consistent, the pair breaking and energy relaxation must be fast compared to the time scale τ_{Δ} of change of Δ . This can be realized only close enough to the transition, or in superconductors with magnetic impurities [3], where the inequality (20) is violated. Except these special situations, however, the Cooper pairs *are not slaved* to the time-dependent $\Delta(t)$, and the dynamics of each pair has to be treated individually, via Eq. (7).

II. BOGOLIUBOV-DEGENNES EQUATION AS A BLOCH EQUATION

To analyze the nonlinear BCS dynamics we reformulate the Bogoliubov approach, bringing it to a form amenable to analytic and numerical treatment. We show that the evolution of time-dependent amplitudes $u_{\mathbf{p}}(t), v_{\mathbf{p}}(t)$, governed by the Bogoliubov-deGennes equation (7) with the selfconsistency condition (6), can be cast in the form of a Bloch equation for auxiliary variables. This is achieved by introducing a new set of variables,

$$f_{\mathbf{p}} = 2u_{\mathbf{p}}v_{\mathbf{p}}^*, \quad g_{\mathbf{p}} = |u_{\mathbf{p}}|^2 - |v_{\mathbf{p}}^*|^2. \quad (21)$$

Applied to the quantities (21), Eq.(7) gives a system of coupled equations:

$$\frac{df_{\mathbf{p}}}{dt} = -2i\epsilon_{\mathbf{p}}f_{\mathbf{p}} + 2i\Delta g_{\mathbf{p}}, \quad \frac{dg_{\mathbf{p}}}{dt} = i\Delta^*f_{\mathbf{p}} - i\Delta f_{\mathbf{p}}^*. \quad (22)$$

These are nothing but the Gorkov equations [29] for the Green's functions G and F . In the form (22), using momentum-dependent quantities $f_{\mathbf{p}}$, $g_{\mathbf{p}}$, these equations were first written by Volkov and Kogan [6].

The dynamics (22) is to be supplemented by the Gorkov selfconsistency relation [29],

$$\Delta = \frac{\lambda}{2} \sum_{\mathbf{p}} f_{\mathbf{p}}, \quad (23)$$

which defines $\Delta(t)$ through the values of evolving $f_{\mathbf{p}}(t)$. The initial conditions

$$f_{\mathbf{p}}^{(0)} = e^{i\phi_{\mathbf{p}}}(1 - n_{\mathbf{p}})n_{\mathbf{p}}, \quad g_{\mathbf{p}}^{(0)} = 1 - 2n_{\mathbf{p}}, \quad (24)$$

correspond to the unpaired Fermi gas state (17).

To gain insight in the behavior of Eqs.(22), it will be convenient to introduce the Bloch representation

$$\mathbf{r}_{\mathbf{p}} = (r_1, r_2, r_3)_{\mathbf{p}}, \quad r_1 + ir_2 = f_{\mathbf{p}}, \quad r_3 = g_{\mathbf{p}}. \quad (25)$$

The norm of $\mathbf{r}_{\mathbf{p}}$ is given by

$$|\mathbf{r}_{\mathbf{p}}| = \sqrt{|f_{\mathbf{p}}|^2 + g_{\mathbf{p}}^2} = n_{\mathbf{p}}^2 + (1 - n_{\mathbf{p}})^2. \quad (26)$$

Remarkably, after rewriting Eq.(22) in terms of $\mathbf{r}_{\mathbf{p}}$, it assumes the form of a Bloch equation:

$$\frac{d\mathbf{r}_{\mathbf{p}}}{dt} = 2\mathbf{b}_{\mathbf{p}} \times \mathbf{r}_{\mathbf{p}}, \quad (27)$$

where the ‘‘magnetic field’’ $\mathbf{b}_{\mathbf{p}} = -(\Delta', \Delta'', \epsilon_{\mathbf{p}})$ has time-dependent x and y component satisfying the selfconsistency condition (23). The norm of the Bloch vectors $\mathbf{r}_{\mathbf{p}}$, given by Eq.(26), is less than one, which describes the effect of Pauli blocking, i.e. decoupling of the states with single occupancy from the BCS dynamics (see Sec.I).

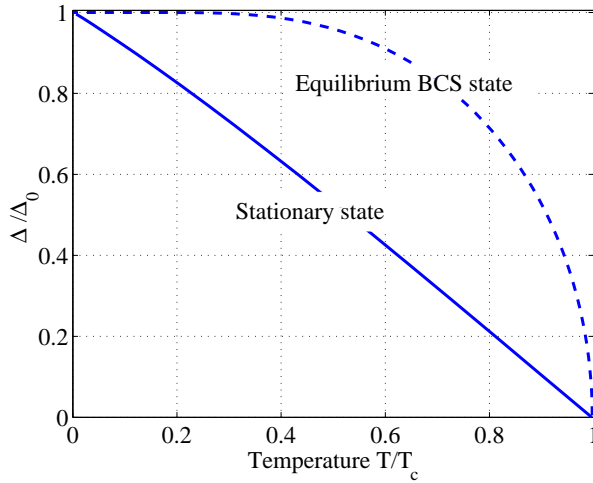


FIG. 2. Temperature dependence of the pairing amplitude Δ for the stationary state (28), (29) obtained from the unpaired state by adiabatic increase of coupling. The equilibrium BCS gap is shown for comparison.

Before exploring the dynamics, let us inspect the stationary states of Eq.(27). The latter are described by the Bloch spins aligned with the magnetic field axis, $\mathbf{l}_{\mathbf{p}} = -\mathbf{b}_{\mathbf{p}}/|\mathbf{b}_{\mathbf{p}}|$. In this case we have

$$(l_1 + il_2)_{\mathbf{p}} = \frac{\Delta}{\sqrt{\epsilon_{\mathbf{p}}^2 + |\Delta|^2}}, \quad l_{3,\mathbf{p}} = \frac{\epsilon_{\mathbf{p}}}{\sqrt{\epsilon_{\mathbf{p}}^2 + |\Delta|^2}}, \quad (28)$$

and the selfconsistency condition (23), which determines the stationary value of Δ , takes the form

$$1 = \frac{\lambda}{2} \sum_{\mathbf{p}} \frac{\tanh(\frac{1}{2}\beta|\epsilon_{\mathbf{p}}|)}{\sqrt{\epsilon_{\mathbf{p}}^2 + |\Delta|^2}}. \quad (29)$$

The numerator, $\tanh(\frac{1}{2}\beta|\epsilon_{\mathbf{p}}|) = |1 - 2n_{\mathbf{p}}|$, is the length of the Bloch vector $\bar{\mathbf{r}}_{\mathbf{p}}$ averaged over a group of levels with nearly equal energies, $|\epsilon_{\alpha} - \epsilon_{\beta}| \ll \Delta$. The averaging, applied to the initial $\mathbf{r}_{\mathbf{p}}$ values (24), eliminates the transverse part of (24), containing random phases $\theta_{\mathbf{p}}$, while leaving the longitudinal part intact. The Bloch dynamics is unitary with respect to each Bloch vector $\mathbf{r}_{\mathbf{p}}$ and, in particular, is linear and preserves the norm. As a result, the averaged vectors $\bar{\mathbf{r}}_{\mathbf{p}}$ will evolve according to the same Bloch equations, albeit having a smaller norm $|\bar{\mathbf{r}}_{\mathbf{p}}| = |1 - 2n_{\mathbf{p}}| < |\mathbf{r}_{\mathbf{p}}|$.

The equation (29) is different from the BCS gap equation which contains $\tanh(\frac{1}{2}\beta(\epsilon_{\mathbf{p}}^2 + \Delta^2)^{1/2})$ instead of $\tanh(\frac{1}{2}\beta|\epsilon_{\mathbf{p}}|)$, except $T = 0$, when these equations coincide since $\tanh = \pm 1$ in both cases. Thus at temperatures $0 < T < T_c$, as Fig.2 illustrates, Eq.(29) predicts the stationary value of Δ below the BCS gap scale. The temperature at which Δ vanishes coincides with the BCS critical temperature, since the condition (29) at $\Delta = 0$ is identical to the BCS equation for T_c .

To clarify the character of the states (28), (29), one can make the following observations. The only difference here from the BCS theory is due to incomplete equilibrium, owing to the singly occupied states being Pauli-blocked from the dynamics controlled by (3). Indeed, the truncated BCS Hamiltonian (3) accounts only for the collisionless pair dynamics, but not for single particle scattering and relaxation. The latter processes have characteristic rates set by the two-particle collisions, $1/\tau_{el}$. Since τ_{el} is larger than $\tau_{\Delta} = \gamma^{-1}$, the approach accounting only for the coherent dynamics, but not for relaxation, is valid in a relatively large time interval $0 < t \lesssim \tau_{el}$.

The stationary nonequilibrium states (28), (29) can be realized when the coupling constant λ increases as a function of time slowly on the scale of τ_{Δ} , i.e. the condition (2) is replaced by

$$\tau_{\Delta} \ll \tau_0 \ll \tau_{el}.$$

In this case, each Bloch vector $\mathbf{r}_{\mathbf{p}}$ follows the direction of the field $\mathbf{b}_{\mathbf{p}}(t)$, maintaining constant projection on the

$\mathbf{b}_{\mathbf{p}}(t)$ axis equal to $1 - 2n_{\mathbf{p}}$ on average. During the evolution, the value $\Delta(t)$ is determined by the selfconsistency condition (23). The amplitudes of the pair states with occupancy zero and two thereby become slaved to the adiabatic dynamics $\Delta(t)$, evolving according to (28), (29). At the same time, the amplitudes with occupancy one remain decoupled, and do not evolve at times $t < \tau_{\text{el}}$. Such a behavior can be seen as a result of the evolution which is simultaneously adiabatic in the pair sector, and totally nonadiabatic in the single particle sector.

III. OSCILLATORY SOLUTIONS, ANALYTICAL AND NUMERICAL

Here we consider the nonlinear BCS dynamics described by the Bloch equation (27) and the selfconsistency relation (23) at the times after the instability sets in. Eq. (27) is quite easy to simulate, since it is linear in $\mathbf{r}_{\mathbf{p}}$ and is written for classical, rather than quantum variables. The initial state, Eq.(24), describing free fermions at a finite temperature, is

$$r_{1,\mathbf{p}} + ir_{2,\mathbf{p}} = \frac{e^{i\phi_{\mathbf{p}}}}{\cosh(\frac{1}{2}\beta\epsilon_{\mathbf{p}})}, \quad r_{3,\mathbf{p}} = \tanh(\frac{1}{2}\beta\epsilon_{\mathbf{p}}), \quad (30)$$

with uncorrelated phases, uniformly distributed in the interval $0 < \phi_{\mathbf{p}} < 2\pi$. This form of initial conditions corresponds to the amplitudes $u_{\mathbf{p}}$, $v_{\mathbf{p}}$ of the form (17). To avoid confusion with temporal characteristics, such as the oscillation period T , hereafter we shall use the inverse temperature β , unless explicitly stated otherwise.

The dynamics (27), (23) was obtained from $3N$ coupled differential equations with the initial conditions (30), with N large enough to ensure proximity to the continual limit. The numerics was executed using the Runge-Kutta method with precision $O(dt^5)$. The time step dt was varied over a range of values to test numerical accuracy. We found that the step $dt = 0.01/\Delta_0$ typically provides sufficient precision over the time interval of interest.

As Fig.3 illustrates, a straightforward simulation generates a surprisingly regular, oscillatory time dependence $\Delta(t)$ which appears to be a periodic function of time. After initial exponential growth, controlled by the instability discussed in Sec.I, we observe an essentially periodic time dependence, characterized by equally spaced peaks of identical shape. We can thus define the temporal period T , the time lag τ , and the amplitude which we denote by Δ_+ for the reasons to become clear below. These notations are marked in Fig.3.

It might seem that the particle-hole symmetry of the density of states (11), (12) would enforce zero chemical potential, regardless of BCS interaction strength. In the simulation, however, we observe nonzero values of chemical potential due to particle-hole imbalance caused by thermal fluctuations in the initial distribution $n_{\mathbf{p}}$. The complex pairing amplitude exhibits a phase growing linearly with time, $\Delta(t) = e^{-i\phi(t)}|\Delta(t)|$, $\phi(t) \propto \omega t$, with

ω random in sign, constant for each realization, equal twice the chemical potential. In addition, we observe noise superimposed on the linear time dependence of the phase, which we shall discuss below at the end of this section. As noted in Ref. [5], finite ω can be eliminated by a gauge transformation which shifts single particle energies by $\omega/2$, $\tilde{\epsilon}_{\mathbf{p}} = \epsilon_{\mathbf{p}} - \omega/2$, thereby making Δ real. In the Bloch equation language, this is equivalent to considering the problem in a Larmor frame rotating about the $\hat{\mathbf{z}}$ axis with frequency ω . Having this in mind, below we shall focus on the behavior of the modulus $|\Delta|$.

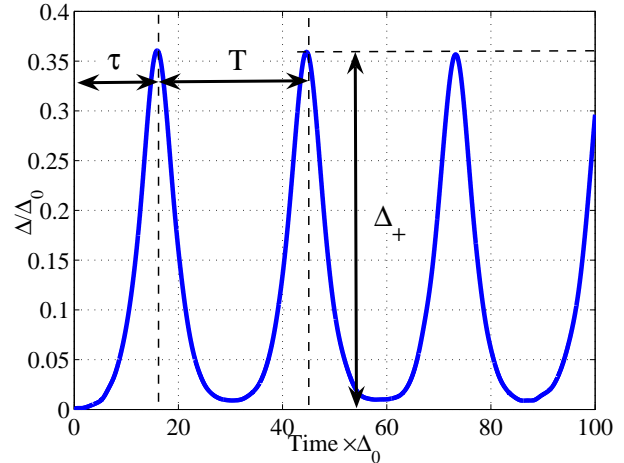


FIG. 3. Time dependence of the pairing amplitude Δ recorded from simulation with $N = 10^5$ states (11), (12) at temperature $T = 0.7T_c$ ($\beta = 2.5\Delta_0$) with the initial conditions (30). The coupling constant λ was chosen to have the BCS gap $\Delta_0 = W/5$.

Interestingly, the obtained time dependence $\Delta(t)$ can be fitted extremely accurately to the analytic solution found in Ref. [5] for noiseless initial conditions. The latter is given by a Jacobi elliptic function, periodic in time,

$$\Delta(t) = \Delta_+ \text{dn}(\Delta_+(t - \tau), k), \quad k^2 = 1 - \Delta_-^2/\Delta_+^2, \quad (31)$$

with Δ_+ the amplitude, τ the time lag, and Δ_- the minimal value. We recall that the function $u = \text{dn}(x, k)$ is obtained by inversion of an elliptic integral:

$$x = \int_u^1 \frac{du'}{\sqrt{(1-u'^2)(k^2-1+u'^2)}} \quad (32)$$

The function (31) satisfies the differential equation

$$(d\Delta/dt)^2 = (\Delta_+^2 - \Delta^2)(\Delta^2 - \Delta_-^2) \quad (33)$$

with Δ_{\pm} being the extremal values: $\Delta_- \leq \Delta(t) \leq \Delta_+$. The period of the function (31) is given by the complete elliptic integral of the 1st kind:

$$T = \frac{2}{\Delta_+} K(k) = \frac{2}{\Delta_+} \int_0^{\pi/2} \frac{d\phi}{\sqrt{1 - k^2 \sin^2 \phi}}. \quad (34)$$

For sparse soliton trains, $T\Delta_+ \gg 1$, this expression simplifies to $T = \frac{2}{\Delta_+} \ln(4\Delta_+/\Delta_-)$.

The time dependence of the Bloch vectors $\mathbf{r}_{\mathbf{p}}(t)$ can be obtained from the ansatz

$$z_{\mathbf{p}} = A_{\mathbf{p}}\Delta(t) + iB_{\mathbf{p}}\dot{\Delta}(t), \quad r_{3,\mathbf{p}} = C_{\mathbf{p}}\Delta^2 - D_{\mathbf{p}}. \quad (35)$$

Eqs.(22) are satisfied by (35) provided $A_{\mathbf{p}} = 2\epsilon_{\mathbf{p}}B_{\mathbf{p}}$ and $B_{\mathbf{p}} = -C_{\mathbf{p}}$. The normalization condition $r_1^2 + r_2^2 + r_3^2 = 1$ thereby turns into Eq.(33), the same for all \mathbf{p} , yielding the relation between $C_{\mathbf{p}}$, $D_{\mathbf{p}}$ and Δ_{\pm} :

$$\frac{D_{\mathbf{p}}^2 - 1}{C_{\mathbf{p}}^2} = \Delta_-^2 \Delta_+^2, \quad 2\frac{D_{\mathbf{p}}}{C_{\mathbf{p}}} = 4\epsilon_{\mathbf{p}}^2 + \Delta_-^2 + \Delta_+^2. \quad (36)$$

Here $C_{\mathbf{p}}$ and $D_{\mathbf{p}}$, and likewise $A_{\mathbf{p}}$ and $B_{\mathbf{p}}$, depend on $\epsilon_{\mathbf{p}}$, while the quantities Δ_{\pm} are the same for all \mathbf{p} .

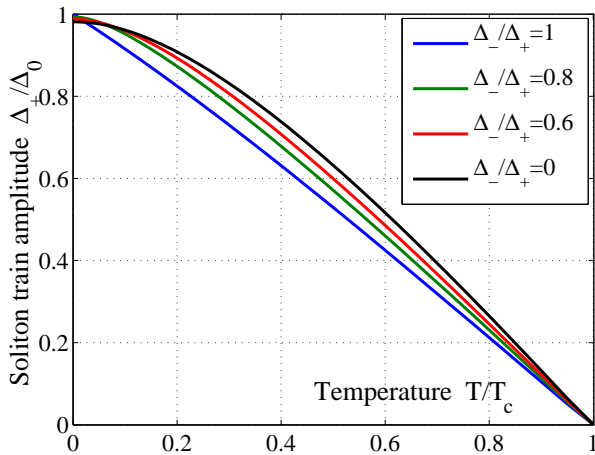


FIG. 4. Temperature dependence of the soliton train amplitude Δ_+ , obtained from the selfconsistency condition (37) at different ratios Δ_-/Δ_+ . Note that at $\Delta_- = 0$ the amplitude Δ_+ equals the BCS instability growth increment γ (see Fig.1), while at $\Delta_- = \Delta_+$ the result for the stationary state is reproduced (see Fig.2).

A special property of the ansatz (35) which makes it compatible with the selfconsistency condition (23), is that $f_{\mathbf{p}} = A_{\mathbf{p}}\Delta(t)$ has the same time dependence as the left hand side of Eq.(23). Therefore, the selfconsistency will hold at all times provided that the quantities Δ_{\pm} are chosen to satisfy $1 = \frac{\lambda}{2} \sum_{\mathbf{p}} |\bar{\mathbf{r}}_{\mathbf{p}}| A_{\mathbf{p}}$. Here the averaging $\bar{\mathbf{r}}_{\mathbf{p}}$ over a group of levels with close energies is performed in the same way as in the derivation of Eq.(29). (As above, the averaging is compatible with unitary evolution due the linear character of Bloch dynamics.) After substituting the expressions for $A_{\mathbf{p}}$ in terms of Δ_{\pm} , and $\bar{\mathbf{r}}_{\mathbf{p}} = 1 - 2n_{\mathbf{p}}$, we obtain

$$1 = \lambda \sum_{\mathbf{p}} \frac{2\epsilon_{\mathbf{p}} \tanh(\frac{1}{2}\beta\epsilon_{\mathbf{p}})}{((4\epsilon_{\mathbf{p}}^2 + \Delta_-^2 + \Delta_+^2)^2 - 4\Delta_-^2\Delta_+^2)^{1/2}}. \quad (37)$$

The role of this equation is similar to the BCS gap equation. The only difference is that it fixes one of the two constants Δ_{\pm} , leaving the other one free.

The motivation to consider this particular solution can be seen from the behavior of the elliptic integral (32) at $\Delta_- = 0$. In this case, we obtain a single soliton

$$\Delta(t) = \frac{\Delta_+}{\cosh \Delta_+(t - t_0)}. \quad (38)$$

At large negative time, Eq.(38) describes exponential growth of Δ . Furthermore, Eq.(37) at $\Delta_- = 0$ is identical to the condition (18) for the instability growth rate, so that $\Delta_+ = \gamma$. Thus the single soliton solution (38) describes the nonlinear evolution following the linear instability regime. The nonmonotonic behavior of $\Delta(t)$, first growing and then decreasing to zero, can be understood as a result of energy mismatch of the BCS ground state and the unpaired state: Energy conservation in the collisionless dynamics prevents system to evolve to the ground state with lower energy.

Remarkably, while these solutions appear to be very special, they are robust in the presence of noise. Below we study the instability of Fermi gas at finite temperature, and find that the time dependence survives thermal fluctuations in the initial state. The reason for such a behavior is owing to the property of BCS instability, discussed in Sec.I, to develop through a single unstable mode. As a result, only the fluctuation in the initial state along the unstable direction is amplified by BCS dynamics, while other fluctuations remain small, providing a selection mechanism for the solutions (37).

Returning to the analysis of soliton trains (31), we note that the ratio $r = \Delta_-/\Delta_+$ controls the inter-soliton time separation. Different regimes can be qualitatively understood by noting that Δ varies in the interval $\Delta_- \leq \Delta(t) \leq \Delta_+$. For r increasing from 0 to 1, the soliton train period T decreases, making the solitons overlap stronger and gradually merge, turning into weak harmonic oscillations with frequency $2\Delta_+$ as Δ_- approaches Δ_+ (see Fig. 1 of Ref. [5]).

As a function of temperature, the quantity Δ_+ varies from the value close to the BCS gap Δ_0 at $T = 0$, to zero at $T = T_c$ (see Fig.4). At $\Delta_- \ll \Delta_+$, Eq. (37) turns into Eq. (10) which, as we found above, defines the amplitude of a single soliton (38). In the opposite limit, $\Delta_- \rightarrow \Delta_+$, Eq. (37) coincides with Eq.(29) for the stationary state.

To understand the behavior of Δ_+ in more detail, let us analyze the selfconsistency condition (37) for the symmetric band of states (12). We first consider zero temperature, when $\tanh \frac{1}{2}\beta\epsilon = \text{sgn } \epsilon$. The integral (37), evaluated using variable substitution $x = 4\epsilon^2$, gives

$$\frac{1}{2} \int_0^{W^2} \frac{dx}{\sqrt{(x + \Delta_+^2 + \Delta_-^2)^2 - 4\Delta_+^2\Delta_-^2}} \quad (39)$$

$$= \cosh^{-1} \frac{W^2 + (r^2 + 1)\Delta_+^2}{2r\Delta_+^2} - \ln \frac{1}{r}. \quad (40)$$

Substituting this in Eq. (37) and solving it, we obtain

$$\Delta_+^2 = \frac{W^2}{2(e^{1/\lambda} - r^2 e^{-1/\lambda}) \sinh \frac{1}{\lambda}}, \quad (41)$$

where here and below the density of states is absorbed in the coupling, $\lambda\nu_0 \rightarrow \lambda$. At $r = 1$ we recover the BCS gap for the symmetric band (12), $\Delta_0 = W/2 \sinh \frac{1}{\lambda}$. At $r < 1$ we obtain a value somewhat below Δ_0 , the difference being small as $(1 - r^2)e^{-2/\lambda} \Delta_0$. This explains small

departure from Δ_0 seen in Figs.1,4 at $T = 0$, as well as its absence in Fig.2.

The simulated dynamics $\Delta(t)$ appears to be periodic (or very close to it) over the entire time interval of the simulation. A nearly perfect fit to $\Delta(t)$, as illustrated in Figs.5,6, is provided by the elliptic function (31) with the same period and amplitude. The numerical and analytic functions are found to agree to accuracy better than 10^{-4} for $\beta = 100/\Delta_0$ (Fig.5 inset, top panel) and 10^{-3} for $\beta = 10/\Delta_0$ (Fig.6 inset, top panel).

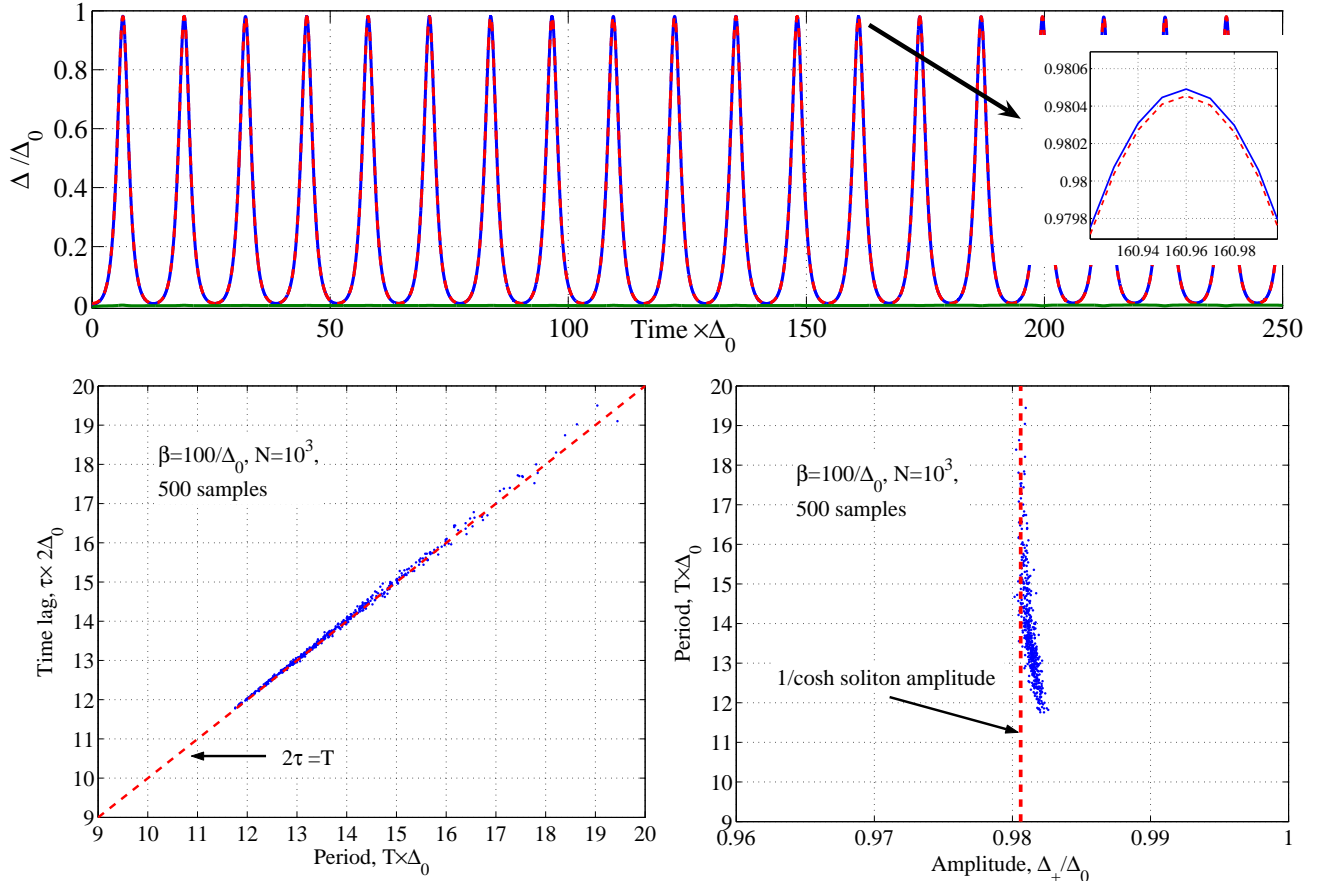


FIG. 5. *Top panel:* Comparison of the time dependence $\Delta(t)$ obtained from BCS/Bloch dynamics (27), (23) for $N = 10^3$ spins at temperature $T = 10^{-2}\Delta_0$ (blue curve) to the analytic soliton train solution (31) of the same amplitude and period (green curve). The difference of the simulated and analytic $\Delta(t)$ is shown in red. (The initial conditions (30) and parameters W , Δ_0 are the same as in Fig.3.) *Lower panels:* The pair distributions of the soliton train parameters for 500 different realizations: the time lag and period (left); the period and amplitude (right).

While each realization $\Delta(t)$ is essentially a perfectly periodic function of time of the form (31), the parameters such as the period T , the time lag τ , and the amplitude Δ_+ exhibit significant variations from one realization to another. To explore this phenomenon, we generated a large number (500) of different realizations, and for each of them determined the values T , τ and Δ_+ from fitting to the elliptic function (31). Figs.5,6 display the result-

ing pair distributions as a set of points in the (T, τ) and (T, Δ_+) planes, one point per realization.

These results lead to a number of interesting observations. First, as one would expect, the distribution is less noisy at lower temperature (Fig.5). Second, while at $\beta = 10/\Delta_0$ the points are scattered over a 2d region, at $\beta = 100/\Delta_0$ each distribution collapses on a 1d curve, indicating a specific relation between T , τ and Δ_+ at the

lower temperature.

The pair distribution of the period and the time lag tends to cluster around the straight line

$$\tau = T/2. \quad (42)$$

This can be understood from the linear stability analysis of Sec.I. Indeed, there we found that the linearized BCS problem has only two eigenvalues outside the unit circle, $\zeta = \omega + i\gamma$ and $\zeta^* = \omega - i\gamma$. The projections of the initial unpaired state on these two vectors are close by order of magnitude. Now, let us take into account that the elliptic function (31) at large period $T\Delta_+ \gg 1$ represents a train of well-separated $1/\cosh$ solitons (38):

$$\Delta(t) = \sum_n \frac{\Delta_+}{\cosh \Delta_+(t - t_n)} + O(e^{-\gamma T}), \quad \Delta_+ = \gamma, \quad (43)$$

$t_n = nT + \tau$. In between the solitons this function is given by a sum of exponential tails of the nearest solitons:

$$\Delta(t_n \lesssim t \lesssim t_{n+1}) = \gamma(e^{-\gamma(t-t_n)} + e^{\gamma(t-t_{n+1})}).$$

The amplitudes of the two terms, taken at some t in the interval (t_n, t_{n+1}) , should match the ζ, ζ^* projections of the initial state for the numerical and analytical solution to coincide. Since the terms $e^{-\gamma(t-t_n)}, e^{\gamma(t-t_{n+1})}$ are equal at the midpoint $t_0 = \frac{1}{2}(t_n + t_{n+1})$, the time t defined by the matching condition must be close to t_0 . This suggests that the time lag τ should indeed be close to half a period, with the product $(2\tau - T)\gamma$ of order one and random in sign. This conclusion is consistent with our observations at different temperatures (Figs.5,6).

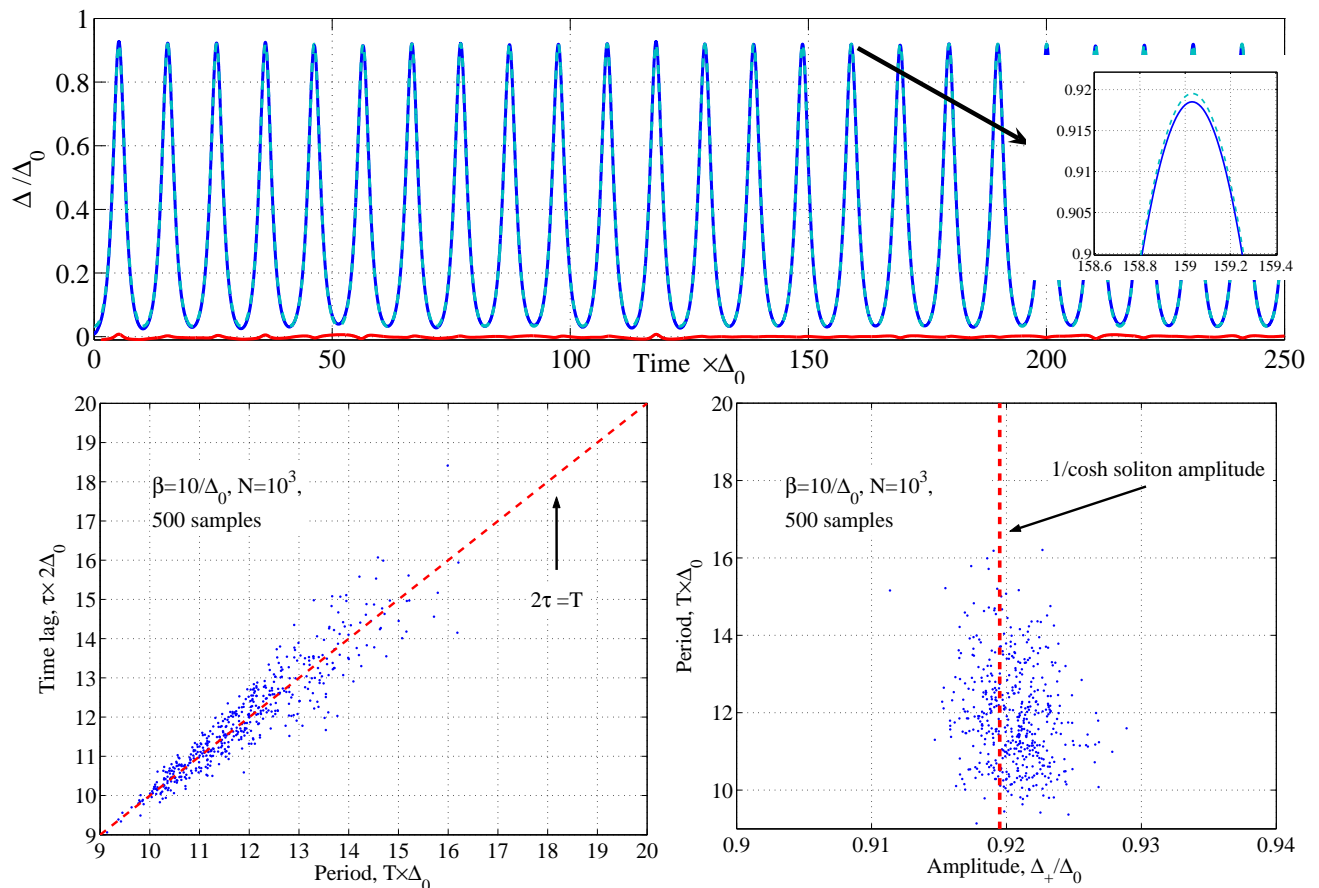


FIG. 6. Same as in Fig.5 for higher temperature $T = 10^{-1} \Delta_0$. The simulated time dependence $\Delta(t)$ can be accurately fitted to the analytic solution (31), with the distribution of the period, amplitude and time lag somewhat broader than in Fig.5.

To complete the description of the behavior of Δ , obtained in simulation, here we analyze the phase dynamics. The phase $\phi = \arg \Delta(t)$ recorded in the simulation exhibits an approximately linear time dependence, as illustrated in Fig.7. As discussed above, in a system with

perfect particle-hole symmetry one expects the chemical potential to be pinned to the band center, in which case the condition $d\phi/dt = 2\mu = 0$ would make the phase time-independent. The observed linear behavior can be explained by particle-hole imbalance due to fluctuations

of particle distribution $n_{\mathbf{p}}$ in the initial state. These fluctuations result in nonzero chemical potential of random sign. The fluctuations in μ caused by random occupancy will be estimated in Sec.IV, Eq.(50.ii). The magnitude and temperature dependence of the fluctuations is found to be consistent with observations.

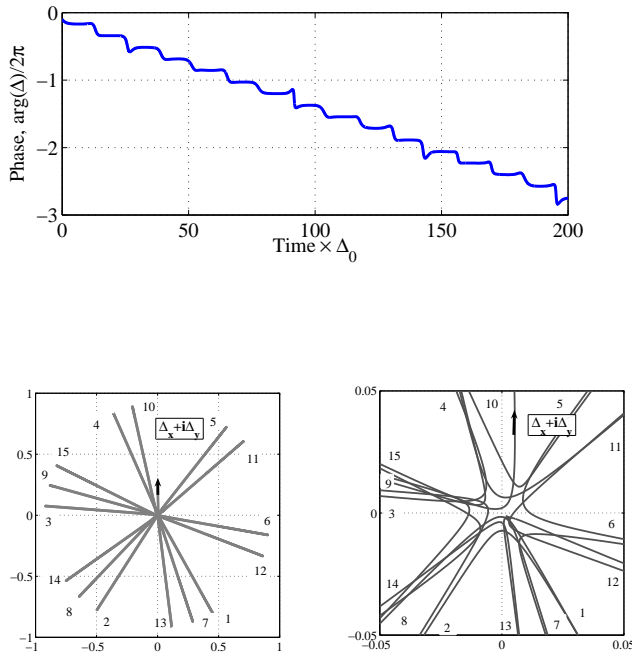


FIG. 7. *Top*: The phase of the pairing amplitude *versus* time for the soliton train in Fig.6. *Bottom*: Pairing amplitude $\Delta(t) = \Delta_x(t) + i\Delta_y(t)$ trajectory in the complex plane. The phase $\arg \Delta(t)$ is a linear function of time superimposed with noise. Each radial line in the left panel corresponds to a soliton, marked according to their order in the time sequence. Phase shift between solitons translates into rotation by a constant angle. The right panel shows the behavior near the origin, allowing to trace the order of different solitons.

The noise superimposed on the linear time dependence $\phi(t)$ has several interesting features. First, the fluctuations about the linear dependence show no sign of phase diffusion, since $\delta\phi$ does not grow. Instead, they can be described as a periodic, or quasiperiodic, arrangement of steps connected by kinks. By comparing to Fig.6 which depicts $|\Delta|$ for this simulation, we see that each step is associated with a soliton, while the kinks occur in between the solitons. This behavior can be partially understood by analyzing the trajectory $\Delta(t)$ in a complex plane, displayed in Fig.7. Each radial straight line in this plot corresponds to a soliton, making it apparent that the phase variation occurs mainly in between the solitons. Interestingly, the deviation of the phase time dependence from

linear does not lead to noticeable deviation in $|\Delta|$ from the elliptic function time dependence.

IV. NOISE DUE TO OCCUPANCY FLUCTUATIONS

The robustness of the elliptic function (31) accompanied by sometimes significant variations of the parameters T , τ and Δ_+ among different realizations may seem surprising. To get insight into the origin of this behavior we consider variations in the initial conditions, which can be attributed to fluctuations of the pair states occupancy (15) at $t = 0$. The latter is due to thermodynamic fluctuations of fermion occupancy $n_{\mathbf{p}}$, and can be interpreted more intuitively as temperature fluctuations.

The first thing we note is that the existence of the soliton solutions, as well as their analytic form, is not dependent upon the details of the energy distribution $n_{\mathbf{p}}$, provided the state is unpaired, i.e. there is no coherence in the amplitudes $u_{\mathbf{p}}$, $v_{\mathbf{p}}$ at different \mathbf{p} . The main difference arising for the more general distribution is possible lack of particle-hole symmetry relative to E_F . In this case, the pairing interaction shifts the chemical potential which manifests itself as a time-dependent phase factor $e^{-i\omega t}$ multiplying $\Delta(t)$. As discussed in Ref. [5], this can be taken into account by a gauge transformation which shifts single particle energies by $\omega/2$. In the transformed problem, only the modulus $|\Delta|$ varies with time, with its functional form still given by the elliptic function (31). The parameters Δ_{\pm} and ω satisfy algebraic selfconsistency equations [5] with $\tanh \frac{1}{2}\beta\epsilon_{\mathbf{p}}$ replaced by $1 - 2n_{\mathbf{p}}$.

The variation in the period T can be linked to the fluctuations in the initial state projection on the unstable mode (9). Denoting this projection η , we can write for it a distribution of Porter-Thomas form [30],

$$P(|\eta| = x) = 2ux \exp(-ux^2), \quad (44)$$

The latter describes fluctuations of individual components of a random complex vector in a high dimensional space, with the parameter u being a function of the vector norm statistics. In our case, the effective dimensionality can be estimated as a ratio of temperature to the level spacing, $d \simeq 1/\beta\delta\epsilon = N/(\beta W)$. To relate η to the period T , we write the time-dependent Δ at the times described by linear instability as $\Delta(t) \propto \eta e^{\gamma t}$. The corresponding time range can be estimated from the condition $\Delta(t) \lesssim \Delta_+ \simeq \gamma$, giving $t = \gamma^{-1} \ln \gamma/\eta$. The time t is close to the phase lag τ which, for the reasons discussed above, is approximately equal to $\frac{1}{2}T$.

Porter-Thomas distribution predicts order of magnitude fluctuations with typical $\eta \sim u^{-1/2}$. This translates into fluctuations of $T = 2\gamma^{-1} \ln \gamma/\eta$ about its mean value with the dispersion independent of u . Indeed, Figs.5,6 indicate that a ten-fold increase in temperature, while reducing the period, has little effect on its fluctuations.

To see whether the randomness in the initial state, and specifically in the occupancy $n_{\mathbf{p}}$, can explain the fluctu-

ations in Δ_+ recorded in Figs.5,6, we consider instability of a particular initial unpaired state (15). Eq.(18) gives an equation for the instability exponent:

$$1 = \lambda \sum_{\mathbf{p}} \frac{g_{\mathbf{p}}}{2\epsilon_{\mathbf{p}} - \zeta}, \quad g_{\mathbf{p}} = |u_{\mathbf{p}}^{(0)}|^2 - |v_{\mathbf{p}}^{(0)}|^2, \quad (45)$$

with microscopic non-averaged $u_{\mathbf{p}}^{(0)}$, $v_{\mathbf{p}}^{(0)}$ taking values zero or one with the probabilities $p_{|u_{\mathbf{p}}|^2=1} = (1 - n_{\mathbf{p}})^2$, $p_{|v_{\mathbf{p}}|^2=1} = n_{\mathbf{p}}^2$ [see Eq.(15)].

The fluctuation $\delta g_{\mathbf{p}}$ causes deviation $\delta\zeta$ from the average value $\zeta = i\gamma$. Linearization of (45) gives

$$\delta\zeta \sum_{\mathbf{p}} \frac{\bar{g}_{\mathbf{p}}}{(2\epsilon_{\mathbf{p}} - i\gamma)^2} = - \sum_{\mathbf{p}} \frac{\delta g_{\mathbf{p}}}{2\epsilon_{\mathbf{p}} - i\gamma} \quad (46)$$

with $\bar{g}_{\mathbf{p}} = \tanh \frac{1}{2}\beta\epsilon_{\mathbf{p}}$. We see that both the real and the imaginary part of $\delta\zeta = \delta\zeta' + i\delta\zeta''$ are nonzero, due to the parts of the distribution fluctuation $\delta g_{\mathbf{p}}$ even and odd relative to E_F . The imaginary part $\delta\zeta''$ gives fluctuation in the instability growth exponent γ . The real part $\delta\zeta'$ can be associated with a shift of the chemical potential due to particle-hole imbalance in the pair sector.

We estimate the magnitude of the fluctuations for low temperature $T \ll \Delta_0 \simeq \gamma$, when Eq.(46) is reduced to

$$\delta\zeta = \frac{i}{\gamma} \sum_{\mathbf{p}} (2\epsilon_{\mathbf{p}} - i\gamma) \delta g_{\mathbf{p}}. \quad (47)$$

Separating the real and imaginary part, we obtain

$$\langle \delta\zeta''^2 \rangle = \delta\epsilon \sum_{\mathbf{p}} \frac{4\epsilon_{\mathbf{p}}^2}{\gamma^2} \langle \delta g_{\mathbf{p}}^2 \rangle, \quad \langle \delta\zeta'^2 \rangle = \delta\epsilon \sum_{\mathbf{p}} \langle \delta g_{\mathbf{p}}^2 \rangle. \quad (48)$$

Here the second moment $\langle \delta g_{\mathbf{p}}^2 \rangle$ is given by

$$\langle \delta g_{\mathbf{p}}^2 \rangle = \overline{(|u_{\mathbf{p}}^{(0)}|^2 - |v_{\mathbf{p}}^{(0)}|^2)^2} - \overline{|u_{\mathbf{p}}^{(0)}|^2} \overline{|v_{\mathbf{p}}^{(0)}|^2} \\ = (1 - n_{\mathbf{p}})^2 + n_{\mathbf{p}}^2 - (1 - 2n_{\mathbf{p}})^2 = 2n_{\mathbf{p}}(1 - n_{\mathbf{p}}). \quad (49)$$

To obtain an order of magnitude estimate, we note that the fluctuations $\delta g_{\mathbf{p}}$ are of order one at $|\epsilon_{\mathbf{p}}| \lesssim T$ and exponentially small at $|\epsilon_{\mathbf{p}}| \gg T$. Thus we find

$$(i) \langle \delta\zeta''^2 \rangle \simeq \frac{T^3}{\gamma^2} \delta\epsilon, \quad (ii) \langle \delta\zeta'^2 \rangle \simeq T \delta\epsilon, \quad (50)$$

where $\delta\epsilon = W/N$ is the level spacing.

The $T^{3/2}$ temperature dependence of the fluctuation in γ , Eq.(50.i), can be compared to the distributions of the amplitude Δ_+ presented in Figs.5,6. As we demonstrated above, Δ_+ is numerically close to γ , becoming equal to it in the limit of well-separated solitons (see Fig.4). According to the $T^{3/2}$ law, a ten-fold increase in temperature from $\Delta_0/100$ to $\Delta_0/10$ should lead to the dispersion in γ increase by a factor of 30, which is indeed close to the increase in Δ_+ dispersion seen in Figs.5,6.

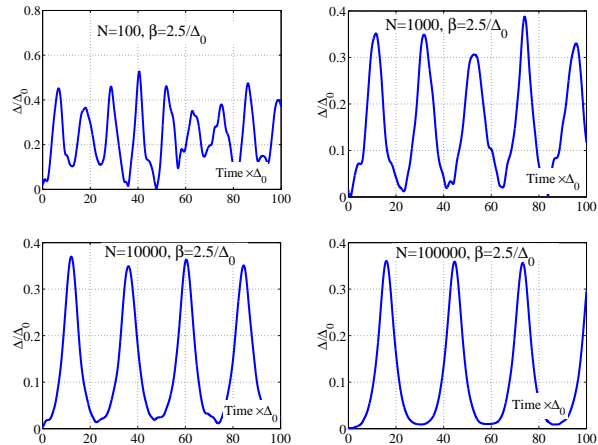


FIG. 8. Noise suppression at increasing number of states N . The time dependence $\Delta(t)$ recorded from a simulation at $T = 0.7T_c$ ($\beta = 2.5\Delta_0$) for $N = 10^2, 10^3, 10^4, 10^5$ states, with other parameters the same as above.

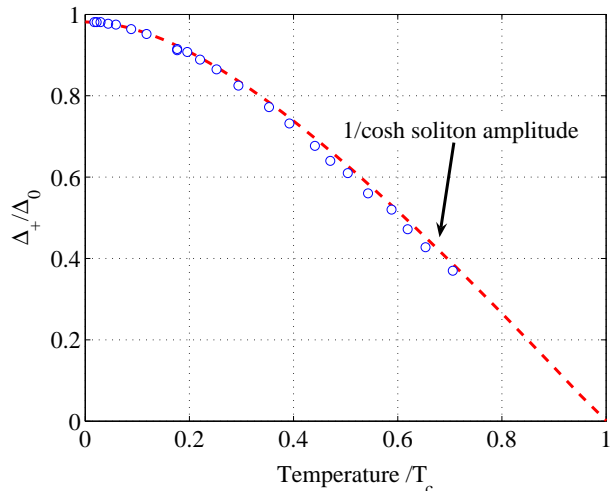


FIG. 9. Temperature dependence of the soliton train amplitude as recorder from the simulation. To suppress noise, the number of levels N was gradually increased from $N = 10$ at the lowest temperature to $N = 10^5$ at the highest temperature. Analytic fit displays the single $1/\cosh$ soliton (38) amplitude obtained from Eq.(37) at $\Delta_- = 0$.

The noise, which quickly grows as a function of temperature, Eq.(50), can be suppressed by reducing the level spacing $\delta\epsilon = W/N$. The dramatic effect of level spacing on noise is illustrated in Fig.8 which presents the time dependent $\Delta(t)$ at a relatively high temperature $T = 0.7T_c$ for several values of the number of levels N . We observe that the noise, at this temperature significant at small N , decreases at large N , with the time dependence assuming the elliptic function form (31). As demonstrated in Fig.9, the soliton train amplitude, recorded at N large enough to minimize noise, follows very closely the analytic temperature dependence, Eq.(37). The value of N required to reduce noise to the level at which the behavior (37) is

revealed, grows as a function of temperature. While at $T = 0$ as few levels as $N = 10$ is quite sufficient, we find that N increases rapidly as T_c is approached.

To analyze the noise at T close to T_c , we again consider fluctuations in the instability growth rate, given by Eq.(46). At these temperatures, since γ is linear in $T_c - T$ near T_c , we have $\gamma \ll T$. In this case, the sum $\sum_{\mathbf{p}} \bar{g}_{\mathbf{p}} (2\epsilon_{\mathbf{p}} - i\gamma)^{-2}$ in (46) equals

$$4i\gamma \sum_{\mathbf{p}} \frac{\epsilon_{\mathbf{p}} \bar{g}_{\mathbf{p}}}{((2\epsilon_{\mathbf{p}})^2 + \gamma^2)^2} = \frac{i\pi}{8} \beta$$

After averaging over fluctuations $\delta g_{\mathbf{p}} = g_{\mathbf{p}} - \bar{g}_{\mathbf{p}}$, we obtain

$$\langle |\delta\zeta|^2 \rangle = \left(\frac{8T}{\pi} \right)^2 \delta\epsilon \sum_{\mathbf{p}} \frac{\langle \delta g_{\mathbf{p}}^2 \rangle}{(2\epsilon_{\mathbf{p}})^2 + \gamma^2}. \quad (51)$$

Using the expression (49) for $\langle \delta g_{\mathbf{p}}^2 \rangle$ at $|\epsilon_{\mathbf{p}}| \ll T$, we have

$$\langle |\delta\zeta|^2 \rangle = \left(\frac{8T}{\pi} \right)^2 \delta\epsilon \sum_{\mathbf{p}} \frac{\langle \delta g_{\mathbf{p}}^2 \rangle}{(2\epsilon_{\mathbf{p}})^2 + \gamma^2} = \frac{16T^2}{\pi\gamma} \delta\epsilon. \quad (52)$$

By inspecting the right hand side of Eq.(46) we find that the fluctuations in $\delta\zeta''$, the instability growth rate, dominate at T close to T_c , while the fluctuations in $\delta\zeta'$, the chemical potential, are smaller by a factor γ/T . Thus Eq.(52) gives an estimate for the fluctuations in γ and, by the argument used above, also provides an estimate of the noise in the soliton train amplitude Δ_+ .

The condition necessary for the noise (52) to be small, $|\delta\zeta| \ll \gamma$, translates into

$$N \gg \frac{16T^2 W}{\pi\gamma^3}. \quad (53)$$

We see that the minimal level number required to suppress noise grows as $(T_c - T)^{-3}$ near the transition. The fast growth is consistent with the results of simulation presented in Figs. 8,9.

The level number N , which so far was taken to be arbitrary, can be related to other parameters as follows. For a system of size L smaller than the BCS correlation length $\xi = \hbar v_F / \Delta$, which corresponds to a tightly trapped cold gas, N is of the order of the total particle number. This can also be written as a relation of N and particle Fermi momentum: $N \simeq (L p_F / 2\pi\hbar)^3$.

In an infinite system, or in a system of size larger than ξ , one can define an effective N equal to the number of particles in the correlation volume, $N \simeq (\xi p_F / 2\pi\hbar)^3 \approx (E_F / \Delta)^3$. Comparing this to the inequality (53), with the identifications $W = E_F$, $\gamma \simeq \Delta \propto T_c - T$, we obtain a condition $E_F^2 \gg T^2$, nonrestrictive in the entire interval $0 < T < T_c$. Other requirements for the mean field approach are also nonrestrictive: (i) The detuning from transition, $T_c - T$, must be outside the fluctuation region, very narrow at weak coupling; (ii) The collisionless

regime condition $\tau_{\Delta} \ll \tau_{el}$ requires that $T_c - T$ is outside the region described by the time-dependent Ginzburg-Landau equation [3], which is also quite narrow. From this one can conclude that the mean field approach, validated by (53), remains accurate in an infinite system, at least for spatially uniform solutions.

It is not unconceivable that the mean field theory, known to work well in equilibrium at weak coupling, is also valid for the dynamical problem with generic spatially varying Δ . However, an understanding of this question can only be achieved after the role of spatial fluctuations in the BCS instability is clarified [22]. Here most interesting are spatial fluctuations of the phase of Δ , and the properties of vortices, which presently are not understood. If the characteristic length scale of phase fluctuations is of order or larger than the correlation length ξ , which seems likely to be the case, the dynamics of the modulus $|\Delta|$ can be obtained in a local approximation, using the results of this work and ignoring spatial dependence.

V. SPIN 1/2 REPRESENTATION

In Sec.II we derived Bloch equations (27) from Bogoliubov-deGennes equations for $u_{\mathbf{p}}$ and $v_{\mathbf{p}}$, by rewriting them in the form of Gorkov equations for $g_{\mathbf{p}} = |u_{\mathbf{p}}|^2 - |v_{\mathbf{p}}|^2$, $f_{\mathbf{p}} = 2u_{\mathbf{p}}v_{\mathbf{p}}^*$, and then recognizing that these quantities form a three-component Bloch vector. To gain more insight, here we demonstrate a different approach in which spin 1/2 operators and Bloch dynamics appear on an earlier stage. Following Anderson [31], we define pseudospins associated with individual Cooper pair states, by assigning 'Pauli spin' operators $\sigma_{\mathbf{p}}^{\pm} \equiv \frac{1}{2}(\sigma_{\mathbf{p}}^x \pm i\sigma_{\mathbf{p}}^y)$ to each pair of fermion states with opposite momenta as follows

$$\sigma_{\mathbf{p}}^+ = a_{\mathbf{p}\uparrow}^+ a_{-\mathbf{p}\downarrow}^+, \quad \sigma_{\mathbf{p}}^- = a_{-\mathbf{p}\downarrow} a_{\mathbf{p}\uparrow}, \quad (54)$$

and $\sigma_{\mathbf{p}}^z \equiv [\sigma_{\mathbf{p}}^+, \sigma_{\mathbf{p}}^-] = a_{\mathbf{p}\uparrow}^+ a_{\mathbf{p}\uparrow} - a_{-\mathbf{p}\downarrow} a_{-\mathbf{p}\downarrow}^+$. This allows to represent the BCS problem (3) as an ensemble of interacting spins:

$$\mathcal{H} = \sum_{\mathbf{p}}' \epsilon_{\mathbf{p}} \sigma_{\mathbf{p}}^z - 2\lambda \sum_{\mathbf{p}, \mathbf{q}}' \sigma_{\mathbf{p}}^+ \sigma_{\mathbf{q}}^-, \quad (55)$$

where $\sum_{\mathbf{p}}'$ means a sum over the pairs of states $(\mathbf{p}, -\mathbf{p})$. Since all the spins interact with each other equally, the mean field theory here is exact, just like for the BCS problem. The mean field Hamiltonian for each spin is

$$\mathcal{H}_{\mathbf{p}} = \mathbf{b}_{\mathbf{p}} \cdot \sigma_{\mathbf{p}}, \quad \mathbf{b}_{\mathbf{p}} = (-\Delta', -\Delta'', \epsilon_{\mathbf{p}}). \quad (56)$$

Here the z component of the effective field $\mathbf{b}_{\mathbf{p}}$, given by the single particle energy, is spin-specific, while the transverse components, the same for all the spins, satisfy

$$\Delta \equiv \Delta' + i\Delta'' = \lambda \sum_{\mathbf{p}}' \langle \sigma_{\mathbf{p}}^+ \rangle. \quad (57)$$

This dynamical selfconsistency relation for time-dependent Δ and $\sigma_{\mathbf{p}}^{\dagger}$ is identical to the Gorkov equation (23). In the ground state each spin is aligned with $\mathbf{b}_{\mathbf{p}}$, and the spins form a texture near the Fermi surface [31], given by Eq.(28), with spin rotation described by the Bogoliubov angle.

The dynamical problem of interest takes the form of a Bloch equation for the spins,

$$\dot{\sigma}_{\mathbf{p}} = i[\mathcal{H}_{\mathbf{p}}, \sigma_{\mathbf{p}}] = 2\mathbf{b}_{\mathbf{p}} \times \sigma_{\mathbf{p}} \quad (58)$$

with the field $\mathbf{b}_{\mathbf{p}}$ defined selfconsistently by (56),(57). Eq. (58), linearized about the texture state, describes collective excitations of a superconductor with frequency 2Δ [6,31]. Linearized about the unpaired state, Eq. (58) describes the BCS instability (10).

The Hilbert space for the spin Hamiltonian (55) can be constructed in a standard fashion, using the states

$$\{\sigma_{\mathbf{p}}\} = |\dots \uparrow \downarrow \uparrow \downarrow \dots\rangle \quad (59)$$

as basis vectors, where $\sigma_{\mathbf{p}} = \uparrow, \downarrow$ correspond to the fully occupied and empty pair states. The pair states having fermionic occupancy one are to be excluded as they are decoupled from the dynamics (55). The Hilbert space spanned by the states (59) provides a full representation of the Hamiltonian (55).

The spin states (59), which are identical to the many-body pair states (16), provide the most general description of the problem. Here one can note, however, that the mean field relation (57) eliminates dynamical coherence of different spins. This allows to simplify the state, replacing (59) by a product state

$$|\psi\rangle = \bigotimes_{\mathbf{p}} \begin{pmatrix} v_{\mathbf{p}} \\ u_{\mathbf{p}} \end{pmatrix}. \quad (60)$$

Comparing this to the fermionic product states (5), (15), we see that the spinor components $u_{\mathbf{p}}, v_{\mathbf{p}}$ are identical to Bogoliubov amplitudes, since the Bogoliubov-deGennes dynamics (7) is equivalent to the Bloch dynamics (58).

One can reduce the spin 1/2 Bloch equations (58) to the Bloch equations (27) for classical vectors $\mathbf{r}_{\mathbf{p}}$ used above as follows. Each pair state $(\mathbf{p}, -\mathbf{p})$ participates in the product (60) with the probability $n_{\mathbf{p}}^2 + (1 - n_{\mathbf{p}})^2$, and is excluded with the probability $2n_{\mathbf{p}}(1 - n_{\mathbf{p}})$. Since the Bloch equation (58) is linear in $\sigma_{\mathbf{p}}$, it takes the same form when $\sigma_{\mathbf{p}}$ is replaced by its expectation value $\mathbf{r}_{\mathbf{p}} = \langle \sigma_{\mathbf{p}} \rangle$. One can include the probability of having occupancy 0 or 2 is the expectation value, which makes the norm of $\mathbf{r}_{\mathbf{p}}$ equal $n_{\mathbf{p}}^2 + (1 - n_{\mathbf{p}})^2$, in agreement with Eq.(26). Thus we see that the spin formulation is indeed equivalent to the fermionic formulation employed above.

VI. DISCUSSION

This work demonstrates that the unpaired fermionic state, after being suddenly presented with pairing inter-

action, develops a BCS instability which triggers oscillations of the pairing amplitude and other quantities. The oscillations are periodic in time and are not damped as long as particle collisions do not play a role. The oscillatory behavior comes quite naturally, given that without collisions the system cannot lower its energy to that of the BCS ground state.

What comes as a surprise, however, is that the oscillations have predictable characteristics despite thermal noise in the initial conditions. The time-dependent pairing amplitude is described by the soliton train solutions of Jacobi elliptic function dn form [5] in which only the parameters such as the period, amplitude and time lag depend on the initial conditions. The explanation for such a behavior can be traced to the physics of the BCS instability. In the latter, when linearization over the unpaired state is analyzed, only one mode exhibits instability, while other modes correspond to the perturbations that do not grow. As a result, in the evolution of a generic unpaired fermion state only the perturbation along the unstable direction is amplified by the instability, selecting the special elliptic function as a time dependence. The accuracy to which the special solution is selected is controlled by the strength of fluctuations in the initial state, due to finite temperature and level spacing.

The selection phenomenon may appear counterintuitive. Here it is instructive to make comparison to the results of Ref. [32] which employs the integrability of the BCS problem to study time-dependent solutions. The large family of solutions obtained in Ref. [32] could leave one under impression that they all are equally relevant for the evolution of a generic state, which does not agree with the results of our simulation and analytic arguments. Instead, as we have seen above, some solutions are singled out by the dynamics, while others are not. This peculiar situation illustrates that knowing the general solution of a nonlinear problem is not necessarily helpful in identifying the special solution relevant for the physical system in which a selection mechanism is at work.

Let us also comment on some issues of interest not considered in this work. One has to do with energy relaxation, left out of the analysis of collisionless BCS dynamics. The relaxation processes relevant for cold gasses are due to elastic collisions involving two particle scattering. The rate of such processes, estimated above as τ_{el}^{-1} , is small compared to the typical frequency of oscillations $\omega \sim \Delta/\hbar$, allowing for undamped oscillations over a relatively long time interval $0 < t \lesssim \tau_{\text{el}}$. While proper treatment of relaxation can only be obtained with the help of quantum kinetic theory, one can account for it heuristically [5] by inserting a Landau-Lifshitz term in the Bloch equation (27), changing $\mathbf{b}_{\mathbf{p}}$ to

$$\mathbf{b}'_{\mathbf{p}} = \mathbf{b}_{\mathbf{p}} - \frac{1}{\tau_{\text{el}}} \mathbf{l}_{\mathbf{p}} \times \mathbf{r}_{\mathbf{p}},$$

where $\mathbf{l}_{\mathbf{p}} = \mathbf{b}_{\mathbf{p}}/|\mathbf{b}_{\mathbf{p}}|$. The resulting evolution exhibits damped oscillations converging to the BCS ground state asymptotically at large times $t \gg \tau_{\text{el}}$.

Another phenomenon of interest is related with spatial fluctuations. Our discussion focused on the dynamics in a system of finite size, of order or smaller than the correlation length, in which we considered spatially uniform $\Delta(t)$, neglecting the spatial dependence altogether. In an infinite system, one expects the emergent pairing dynamics to exhibit phase fluctuations and vortices simultaneously with the oscillations of the modulus $|\Delta|(t)$ similar to that studied above. If the phase fluctuations occur at distances larger than the correlation length and the vortices are dilute, one can use the estimates made at the end of Sec.IV to argue that the modulus $|\Delta|$ will oscillate in a pretty much the same way as in the spatially uniform situation. However, more work will be needed to clarify this.

VII. SUMMARY

In this paper we studied fermionic pairing in a system with time-dependent pairing interaction. We analyze the situation when the pairing builds up after the interaction has been abruptly turned on. Theoretical analysis, supported by numerical simulations, predicts a stage of exponential growth, described by BCS instability of the unpaired Fermi gas, followed by periodic oscillations described by collisionless nonlinear BCS dynamics. We consider spatially uniform situation relevant for systems of small size, and find that:

(i) In the collisionless approximation, at times shorter than the energy relaxation time, the oscillations are undamped;

(ii) The time dependence of the pairing amplitude is obtained from an exact solution of the nonlinear BCS problem [5], a periodic soliton train described by the Jacobi elliptic function dn , with parameters depending on the microscopic initial conditions;

(iii) The robustness of the elliptic function behavior is explained by a dynamical selection process, in which the BCS instability acts to amplify the initial perturbation in a specific unstable mode of the system, generating a time dependence with predictable characteristics;

(iv) The fluctuations of the amplitude, period and time lag of the soliton train can be accounted for by occupation probability fluctuations in the initial state.

ACKNOWLEDGMENTS

This work benefited from discussions with B. Spivak.

APPENDIX A

Here we present yet another derivation of the Bloch equation (27), starting from the evolution of time-dependent amplitudes $u_{\mathbf{p}}(t)$, $v_{\mathbf{p}}(t)$. Let us consider the

Bogoliubov-deGennes equation (7) with the selfconsistency condition (6). By introducing a new variable $w_{\mathbf{p}} = u_{\mathbf{p}}/v_{\mathbf{p}}$, the pair of linear differential equations (7) is reduced to a single nonlinear equation of Riccati form,

$$i\partial_t w_{\mathbf{p}} = 2\epsilon_{\mathbf{p}} w_{\mathbf{p}} + \Delta(t) - \Delta^*(t) w_{\mathbf{p}}^2 \quad (\text{A1})$$

which was analyzed in Ref. [19]. The selfconsistency condition (6), rewritten in terms of $w_{\mathbf{p}}(t)$, becomes

$$\Delta(t) = \lambda \sum_{\mathbf{p}} Q_{\mathbf{p}} \frac{w_{\mathbf{p}}(t)}{1 + |w_{\mathbf{p}}(t)|^2}, \quad (\text{A2})$$

where

$$Q_{\mathbf{p}} = |u_{\mathbf{p}}|^2 + |v_{\mathbf{p}}|^2 \quad (\text{A3})$$

is the norm of $(u_{\mathbf{p}}, v_{\mathbf{p}})$, conserved by the dynamics (7).

The initial value $w_{\mathbf{p}}$ corresponding to the unpaired Fermi gas (17) is $w_{\mathbf{p}}^{(0)} = e^{i\phi_{\mathbf{p}}}(1 - n_{\mathbf{p}})/n_{\mathbf{p}} = e^{\beta\epsilon_{\mathbf{p}} + i\phi_{\mathbf{p}}}$, with the phases $\phi_{\mathbf{p}}$ random and uncorrelated for different \mathbf{p} . For $(u_{\mathbf{p}}, v_{\mathbf{p}})$ of the form (17) we have

$$Q_{\mathbf{p}} = n_{\mathbf{p}}^2 + (1 - n_{\mathbf{p}})^2$$

The factor $Q_{\mathbf{p}} < 1$ describes the effect of Pauli blocking which was discussed in Sec.II.

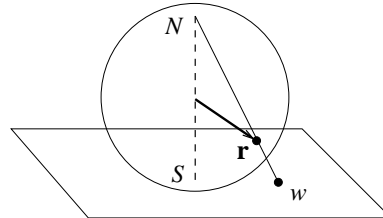


FIG. 10. Stereographic projection (A4) schematic.

The next step is to perform a reverse stereographic projection of the complex variable w , mapping it onto the unit sphere $r_1^2 + r_2^2 + r_3^2 = 1$ as follows:

$$r_1 + ir_2 = \frac{2w}{|w|^2 + 1}, \quad r_3 = \frac{|w|^2 - 1}{|w|^2 + 1} \quad (\text{A4})$$

(see Fig.10). The dynamics (A1), written in terms of $z = r_1 + ir_2$ and r_3 , gives

$$\frac{dz}{dt} = -2i\epsilon_{\mathbf{p}}z + 2i\Delta r_3, \quad \frac{dr_3}{dt} = i\Delta^*z - i\Delta z^*. \quad (\text{A5})$$

After rewriting Eq.(A5) in terms of $\mathbf{r}_{\mathbf{p}} = (r_1, r_2, r_3)_{\mathbf{p}}$, we again obtain the Bloch equation (27), $\dot{\mathbf{r}}_{\mathbf{p}} = 2\mathbf{b}_{\mathbf{p}} \times \mathbf{r}_{\mathbf{p}}$, with the “magnetic field” $\mathbf{b}_{\mathbf{p}} = -(\Delta', \Delta'', \epsilon_{\mathbf{p}})$.

The selfconsistency condition (A2) takes the form

$$\Delta = \frac{\lambda}{2} \sum_{\mathbf{p}} Q_{\mathbf{p}} z_{\mathbf{p}}. \quad (\text{A6})$$

The difference in the form of the selfconsistency relations (A6 and (23)) is due to the difference in normalization of $\mathbf{r}_{\mathbf{p}}$ here and in Sec.II. Here we have $|\mathbf{r}_{\mathbf{p}}| = 1$, while in Sec.II we had $|\mathbf{r}_{\mathbf{p}}| = n_{\mathbf{p}}^2 + (1 - n_{\mathbf{p}})^2 < 1$ which is precisely the factor $Q_{\mathbf{p}}$ needed to account for the difference in the norm.

APPENDIX B

Here we estimate the direct heating of the Fermi system due to the shakeup caused by interaction switching

$$\mathcal{H}_{\text{int}}(t) = \lambda(t) \sum_{p_1+p_2=p_3+p_4} a_{\mathbf{p}_4,\alpha}^+ a_{\mathbf{p}_3,\beta}^+ a_{\mathbf{p}_2,\beta} a_{\mathbf{p}_1,\alpha}.$$

The interaction time dependence during switching is step-like, varying from 0 to λ over a characteristic time τ_0 , so the Fourier component $\lambda_\omega = \int e^{i\omega t} \lambda(t) dt$ behaves as ω^{-1} at $\omega\tau_0 \ll 1$. For example, the interaction switching model $\lambda(t) = \lambda(1 - e^{-t/\tau_0})\theta(t)$ gives $\lambda_\omega = i\lambda/(\omega(1 - i\omega\tau_0))$.

The effective temperature T_{eff} after switching can be estimated from the Golden Rule transition rate for particle energy excitation matched by the net energy increase and fermion specific heat:

$$aT_{\text{eff}}^2 = \sum_{\omega, 1\dots 4} \hbar\omega n_1 n_2 (1 - n_3)(1 - n_4) |\lambda_\omega|^2 \times \delta(\hbar\omega - \epsilon_{\mathbf{p}_3} - \epsilon_{\mathbf{p}_4} + \epsilon_{\mathbf{p}_1} + \epsilon_{\mathbf{p}_2}) \quad (\text{B1})$$

with $n_i = n_{\mathbf{p}_i}$ the occupation numbers of the states $\mathbf{p}_{1\dots 4}$, $a = \frac{\pi^2}{6}\nu$. At $T = 0$, we obtain $aT_{\text{eff}}^2 = \sum_{\omega>0} \hbar\omega N_\omega |\lambda_\omega|^2$ with $N_\omega = \frac{1}{6}\nu^4\omega^3$.

The integral over ω gives $T_{\text{eff}}^2 \simeq \lambda^2 \nu^3 \tau_0^{-3}$. Comparing T_{eff} to Δ_0 we find that the system is not overheated, $T_{\text{eff}} \ll \Delta_0$, when $E_F \tau_0 \gg (\lambda n / \Delta_0)^{2/3}$. This condition is compatible with the nonadiabaticity requirement $\tau_0 \ll \tau_\Delta$, allowing for a range of possible values of the switching times τ_0 for which heating of the Fermi gas is negligible.

[1] D. N. Langenberg, A. I. Larkin, eds., *Nonequilibrium Superconductivity*, Modern Problems in Condensed Matter Sciences, v.12, North-Holland (Amsterdam, New York, 1986)

[2] M. Tinkham, *Introduction to Superconductivity*, (McGraw-Hill, 1996)

[3] L. P. Gor'kov, G. M. Eliashberg, Zh. Eksp. Teor. Fiz. **54**, 612 (1968) [Sov. Phys. JETP **27**, 328 (1968)]

[4] A. G. Aronov, Y. M. Galperin, V. L. Gurevich and V. I. Kozub, Adv. Phys. **30**, 539 (1981)

[5] R. A. Barankov, L. S. Levitov and B. Z. Spivak, Phys. Rev. Lett. **93**, 160401 (2004), cond-mat/0312053

[6] A. F. Volkov and Sh. M. Kogan, Zh. Eksp. Teor. Fiz. **65**, 2038, (1973) [Sov. Phys. JETP, **38**, 1018 (1974)]

[7] A. Schmid, Phys. Kond. Mat. **5**, 302 (1966)

[8] E. Abrahams and T. Tsuneto, Phys. Rev. **152**, 416 (1966)

[9] Yu. M. Gal'perin, V. I. Kozub, and B. Z. Spivak, Sov. Phys. JETP, **54**, 1126 (1981)

[10] B. DeMarco, *et al.*, Phys. Rev. Lett. **82**, 4208 (1999); Science **285**, 1703 (1999); Phys. Rev. Lett. **86**, 5409 (2001); Phys. Rev. Lett. **88**, 040405 (2002).

[11] A. G. Truscott *et al.*, Science **291**, 2570 (2001).

[12] T. Loftus *et al.*, Phys. Rev. Lett. **88**, 173201 (2002).

[13] K. M. O'Hara, *et al.*, Science **298**, 2179 (2002); Phys. Rev. A **66**, 041401 (2002)

[14] C. A. Regal, *et al.* Phys. Rev. Lett. **92**, 040403 (2004)

[15] J. Kinast, *et al.* Phys. Rev. Lett. **92**, 150402 (2004)

[16] M. W. Zwierlein, *et al.* Phys. Rev. Lett. **92**, 120403 (2004)

[17] M. Houbiers and H. T. C. Stoof, Phys. Rev. A **59**, 1556 (1999)

[18] R. A. Barankov and L. S. Levitov, Phys. Rev. Lett. **93**, 130403 (2004)

[19] M. H. S. Amin, E. V. Bezuglyi, A. S. Kijko, and A. N. Omelyanchouk, Low Temp. Phys. **30**, 661 (2004), cond-mat/0404401

[20] A. V. Andreev, V. Gurarie, and L. Radzihovsky Phys. Rev. Lett. **93**, 130402 (2004)

[21] M. H. Szymanska, B. D. Simons, and K. Burnett, Phys. Rev. Lett. **94**, 170402 (2005), cond-mat/0412454

[22] G. L. Warner and A. J. Leggett, unpublished.

[23] E. A. Yuzbashyan, private communication.

[24] T. Akazaki, H. Takayanagi, J. Nitta, and T. Enoki, Appl. Phys. Lett. **68**, 418 (1996)

[25] A. F. Volkov, H. Takayanagi, Phys. Rev. **B53**, 15162 (1996)

[26] T. Schapers, J. Malindretos, K. Neurohr, *et al.*, Appl. Phys. Lett. **73**, 2348 (1998)

[27] A. F. Morpurgo, T. M. Klapwijk, B. J. van Wees, Appl. Phys. Lett. **72**, 966 (1998)

[28] J. Kutchinsky, R. Taboryski, C. B. Sorensen, *et al.*, Phys. Rev. Lett. **83**, 4856 (1999)

[29] L. P. Gor'kov, Zh. Exp. Teor. Fiz. **34**, 735 (1958) [Sov. Phys. JETP **7**, 505 (1958)]

[30] C. Porter and R. Thomas, Phys. Rev. **104**, 483 (1956)

[31] P. W. Anderson, Phys. Rev. **112**, 1900 (1958)

[32] E. A. Yuzbashyan, B. L. Altshuler, V. B. Kuznetsov, and V. Z. Enolskii, cond-mat/0407501 and cond-mat/0505493